

Jason C. Knievel* and Richard H. Johnson
Colorado State University, Fort Collins, Colorado

1. INTRODUCTION

Mesoscale convective systems (MCSs) with leading convective lines and trailing stratiform regions impose upon the troposphere their own mesoscale circulations. These circulations often extend well beyond the clouds and precipitation of an MCS (Menard and Fritsch 1989).

Convectively-generated gravity waves and buoyancy rolls are the agents that transmit an MCS's circulations farthest (Mapes 1993). Gravity waves and buoyancy rolls are propagative; an MCS also generates advective circulations. Among them are a mesoscale updraft and downdraft (e.g., Houze et al. 1989), divergent outflows in the lower and upper troposphere (e.g., Maddox et al. 1981; Cotton et al. 1989), and, in some cases, mesoscale convective vortices (MCVs). MCVs are less common advective circulations, but well more than a dozen may form annually in the central U.S. (Trier et al. 2000).

In this paper we explore the kinematics of an MCS and MCV that traversed the densest part of the National Oceanic and Atmospheric Administration Wind Profiler Network (NPN) in Kansas and Oklahoma on 1 August 1996. Our investigation has two important features: 1) it discriminates between synoptic background wind and a mesoscale perturbation to that wind, and 2) it encompasses nine hours of the system's lifetime.

2. DATA AND METHODS

Satellite data are from channels one (visible), three (water vapor), and four (infrared) from Geostationary Operational Environmental Satellite (GOES) 8.

Radar data are composite base-scan reflectivity with temporal and spatial intervals of 15 min and 2×2 km, as well as level II data from Vance Air Force Base and Oklahoma City, OK.

Kinematical soundings are from the NPN, semi-daily operational radiosondes, and radiosondes launched every three hours as part of 1996's Enhanced Seasonal Observing Period (ESOP-96) of the Global Energy and Water Cycle Experiment's (GEWEX's) Continental-Scale International Project (GCIP).

To produce gridded fields of *total wind* we used a two-pass Barnes analysis (Barnes 1973; Koch et al. 1983) on data from the NPN. Grid points were 75 km apart, and the response function was chosen to capture 90% of the signal of phenomena with wavelengths of 300 km. We then employed a second Barnes analysis that, together with the first, acted as a bandpass filter (Maddox 1980). The *synoptic background wind* was approximated with data filtered to include 90% and 0.09% of the signals of phenomena with wavelengths of 1600 km and 300 km, respectively. The *mesoscale perturbation in wind* was approximated by subtracting the synoptic background wind from the total wind. Therefore, the mesoscale perturbation in wind is environment-relative. (Another paper of ours in this volume provides a graph of the response functions.)

We calculated divergence and vorticity from centered finite differences of gridded wind. Vertical velocity is from the kinematic method with a linear correction to density-weighted divergence (O'Brien 1970), for which we set $w = 0$ at 750 m above the tropopause and $w = 0$ at 500 m above ground level (AGL).

3. OVERVIEW OF THE MCS AND MCV

The MCS of 1 August 1996 epitomized MCSs that generate MCVs. The system formed when three clusters of cumulonimbi merged between 0345 and 0415 UTC (**A**, **B**, and **C** in fig. 1a). For 1 h 15 min the MCS was approximately symmetric about its vector of motion (fig. 1b). Its evolution to asymmetry began at 0715 UTC, when a notch developed at the back of the stratiform region (**N1** in figs. 1c and d) and the convective line bowed into the shape of an *S* (figs. 1c and d). At 1100 UTC the right half of the MCS overtook in western Oklahoma a broad and seemingly unorganized north-south band of cumulonimbi (fig. 1e). (*Right* and *left* are from the perspective of the advancing MCS.) Between 1145 and 1530 UTC a second notch formed at the back of the MCS (**N2** in figs. 1f and g). Then reflectivity on the MCS's far left took on the shape of a hammer head (fig. 1g), and the stratiform region broke into spiral bands. From 1545 UTC on 1 August through 0315 UTC on 2 August, the spiral bands slowly dissipated, and scattered new cumulonimbi grew in the remnants of the bands (fig. 1h).

*Addresses of the corresponding author: Jason C. Knievel, Department of Atmospheric Science, Colorado State University, Fort Collins, CO 80523-1371; knievel@atmos.colostate.edu

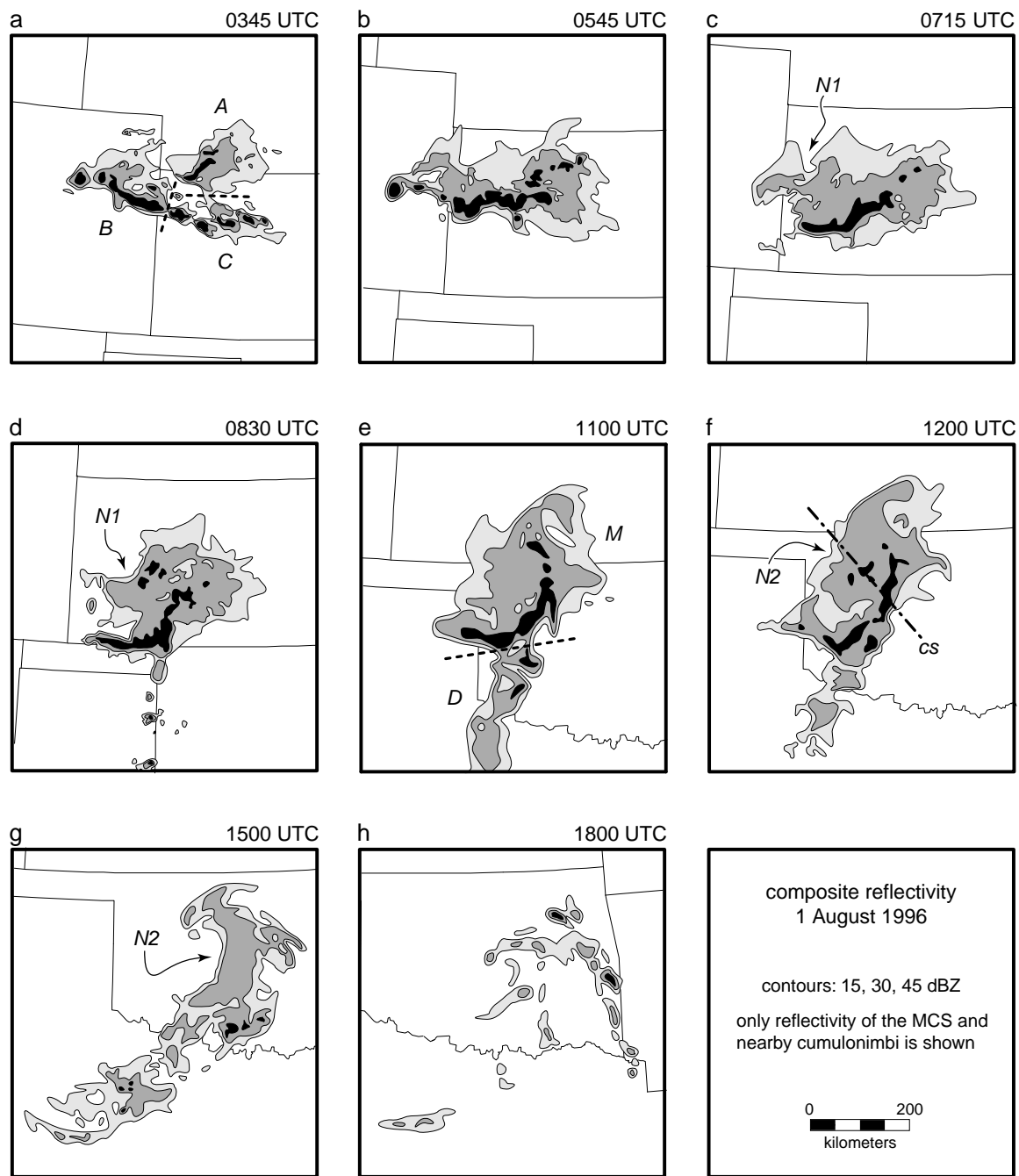


Figure 1: Schemata of composite base-scan radar reflectivity on 1 August 1996. Times are a) 0345, b) 0545, c) 0715, d) 0830, e) 1100, f) 1200, g) 1500, and h) 1800 UTC. Contours are of 15, 30, and 45 dBZ. Only reflectivity due to the MCS and nearby cumulonimbi is shown. Clusters that merged to form the MCS are separated by dashed lines and marked by *A*, *B*, and *C*. A band of cumulonimbi overtaken by the MCS, *M*, is marked by *D*; the two are separated by a dashed line. Notches are marked by *N1* and *N2*. The location of the cross section in figure 2 is marked by *cs*.

4. MESOSCALE PERTURBATION IN WIND

During the MCS's maturity, the mesoscale perturbation in wind (which we occasionally refer to as simply the *mesoscale wind*) included a mesoscale updraft and downdraft, divergent outflow in the lower troposphere, divergent outflow in the upper troposphere, and an MCV centered in the middle troposphere (figs. 2 and 3). Because these circulations appear in the mesoscale perturbation in wind, we conclude that they were internal and fundamental to the MCS of 1 August 1996; they were not merely apparent circulations that resulted from the superposition of the MCS's flow, the environmental flow, and the translational motion of the MCS relative to the environmental flow.

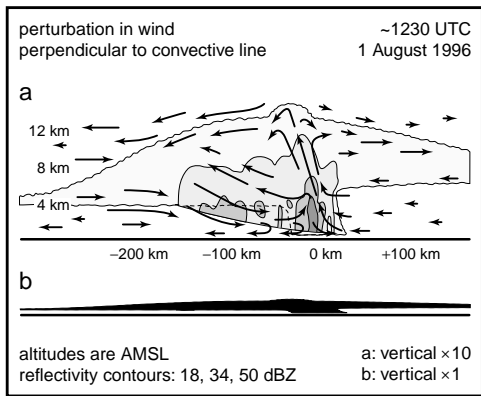


Figure 2: Schematic cross section of reflectivity and the cross-line component of the mesoscale perturbation in wind. Arrows are a hybrid of vectors and streamlines, so their lengths roughly indicate relative wind speed of consistently observed flows along various locations in the MCS as determined from the NPN at 1200 UTC and from cross sections of WSR-88D Doppler velocity from Oklahoma City from 1233 to 1320 UTC. Contours, outer to inner, are of cloud edge and reflectivity of 18, 35, and 50 dBZ. Reflectivity is at 1233 UTC along the cross section shown in figure 1f. The bottom edge of the reflectivity cross section is due to the lower limit of the lowest radar scan. Cloud top is from a GOES 8 IR image at 1215 UTC along the same cross section; cloud bottom is estimated from GCIIP soundings at 1200 UTC and from other studies of MCSs. Height is exaggerated by a factor of ten in the top panel; the bottom panel is an unexaggerated silhouette.

A mesoscale rear inflow jet entered the MCS at the back edge of the stratiform region (fig. 2a), primarily below 8 km above mean sea level (AMSL). This was the rear part of the mesoscale downdraft. Air in the downdraft flowed through the lower part of the anvil and beneath the anvil's base, then descended and overturned, although in some locations there was evidence that the mesoscale downdraft continued toward the front of the MCS, beneath the convective line.

A mesoscale updraft lay above the mesoscale downdraft. The updraft originated at approximately 5 km AMSL along the back edge of the convective line and was at times distinct to an altitude of roughly

10 km AMSL farther than 150 km behind the line. The Coriolis force turned the mesoscale updraft to the right as it ascended, in the manner described by Skamarock et al. (1994) and Scott and Rutledge (1995). The locally fast, divergent, southeasterly flow on the northern side of the MCS at 12 km AMSL appeared to be part of the veering, ascending mesoscale updraft that was exiting the cloud and precipitation of the MCS (fig. 3c).

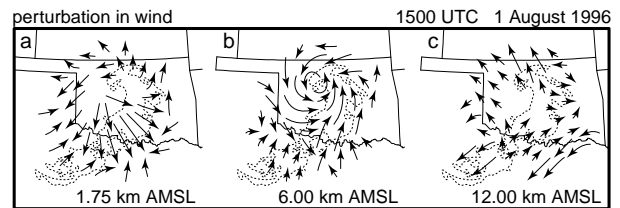


Figure 3: Schemata of the horizontal mesoscale perturbation in wind at 1500 UTC on 1 August 1996. Altitudes are a) 1.75 km, b) 6.00 km, and c) 12.00 km AMSL. Arrows are a hybrid of vectors and streamlines, so their lengths roughly indicate relative wind speed. The contour of 15 dBZ reflectivity within the MCS is dashed.

At 1.75 km AMSL, diverging air beneath and behind falling hydrometeors in the stratiform region converged with environmental air in a ring around the perimeter the MCS's reflectivity (fig. 3a). Convergence in this ring was greatest near the southeastern and southern perimeter. Numerical simulations by Skamarock et al. (1994) demonstrated that such locally maximized convergence on the right side of a convective line characterizes MCSs that mature where the vertical component of planetary vorticity is large.

The magnitude of the mesoscale perturbation in wind was asymmetric about the MCS at some altitudes. In the lower and middle troposphere, the mesoscale perturbation in wind covered a larger area behind the stratiform region than ahead of the convective line (not shown). According to Pandya and Durran (1996) and others, such altitude-dependent asymmetries are symptoms of vertical shear's ability to tilt and horizontally arrange heating and cooling in an MCS. In particular, Pandya and Durran found that in their simulated squall line a deep, rearward-leaning heat source trailed by a heat sink focused the most low-frequency energy in the direction of that tilt.

5. KINEMATICAL AVERAGES OVER THE MCV

Data from the NPN, averaged over 3-h periods and over a $2^\circ \times 2^\circ$ area centered on the MCV in the middle troposphere, reveal the persistent circulations that shaped the MCS and MCV (fig. 4). (References to *vertical velocity*, *divergence*, and *vorticity* in this section are to the temporal and spatial averages of those fields, unless otherwise stated.)

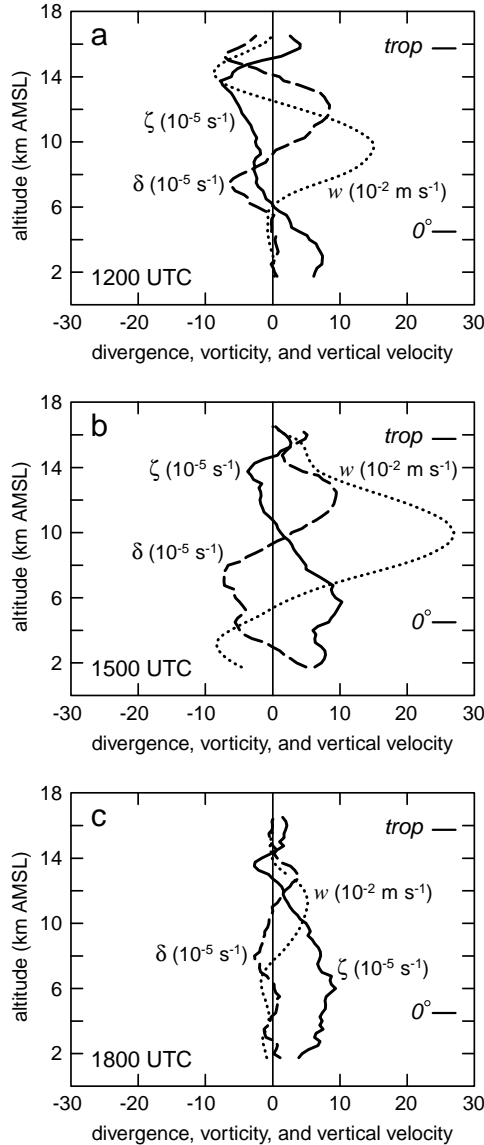


Figure 4: Relative vorticity (solid in 10^{-5} s^{-1}), horizontal divergence (dashed in 10^{-5} s^{-1}), and vertical velocity (dotted in 10^{-2} m s^{-1}) of the total wind on 1 August 1996. Profiles are for a $2^\circ \times 2^\circ$ area centered on the MCV in the middle troposphere, averaged over 3 h ending at the time labeled. The levels of 0°C in the environment and of the tropopause are marked along the right side of each panel.

5.1 Vertical motion and divergence

The four persistent circulations in the stratiform region of the MCS, other than the MCV, were a mesoscale updraft and downdraft that met in a layer of convergence in the middle troposphere, and divergent outflows in both the lower and upper troposphere.

Profiles of vertical motion in figure 4 are signatures of the mesoscale updraft and downdraft. Throughout the nine hours of analysis, divergence in the upper troposphere varied with the mesoscale updraft, whereas

divergence in the lower troposphere varied with the mesoscale downdraft. The mesoscale updraft preceded the mesoscale downdraft (cf. figs. 4a and b), but by the time vorticity in the MCV reached its maximum at 1500 UTC, both mesoscale drafts were present and strong (fig. 4b). Air diverged in the upper troposphere where the mesoscale updraft decelerated, and it diverged in the lower troposphere where the mesoscale downdraft decelerated. The two sloping mesoscale drafts horizontally converged in the middle troposphere (fig. 2a), near the altitude of 0°C in the environment, which is consistent with studies by Houze et al. (1989), Scott and Rutledge (1995), and others.

Unrepresentative data at 1800 UTC, maybe from convective updrafts in a few fresh cumulonimbi, corrupted the average vertical velocity between 1500 and 1800 UTC, so changes in the mesoscale drafts are not accurately conveyed by figure 4c. The more representative profiles at 1700 UTC alone—not averaged over 3 h—show in the decaying MCV only a lingering, deep mesoscale downdraft (fig. 5b).

5.2 Vorticity

Over the nine hours we examined, the MCV deepened and strengthened as the MCS matured and dissipated, until the vortex reached to within a few kilometers of the tropopause (fig. 4).

Positive vorticity in the vortex originated at about 3 km AMSL (fig. 5a), the altitude of its maximum from 0900 to 1200 UTC (fig. 4a). The top of the MCV and the altitude of maximum vorticity both ascended between 1200 and 1500 UTC as the vortex strengthened (fig. 4b). Then the height of maximum vorticity remained near 6 km AMSL for the rest of the analysis period (fig. 4c). The simulated MCV of Zhang and Fritsch (1988) behaved similarly: the height of maximum vorticity varied little for the first 2 h of the MCV's lifetime, rose quickly as the MCV strengthened, then varied little after that. Conversely, Chen and Frank (1993) simulated an MCV whose vorticity maximum descended, not ascended, with time. Few empirical studies recount temporal variations in MCVs' vorticity, but among these few Menard and Fritsch (1989) did find that maximum vorticity ascended with time in the MCV of 6–7 July 1982; this was the MCV simulated by Zhang and Fritsch (1988).

It is not surprising that the MCV of 1 August 1996 grew stronger even while the overall MCS decayed. Although the strength and areal extent of radar echoes in the convective line decreased beginning as early as 1145 UTC, the stratiform region remained vigorous until 1430 UTC (fig. 1), and it is heating in the stratiform region, not heating in the convective line, that generates MCVs (Hertenstein and Schubert 1991).

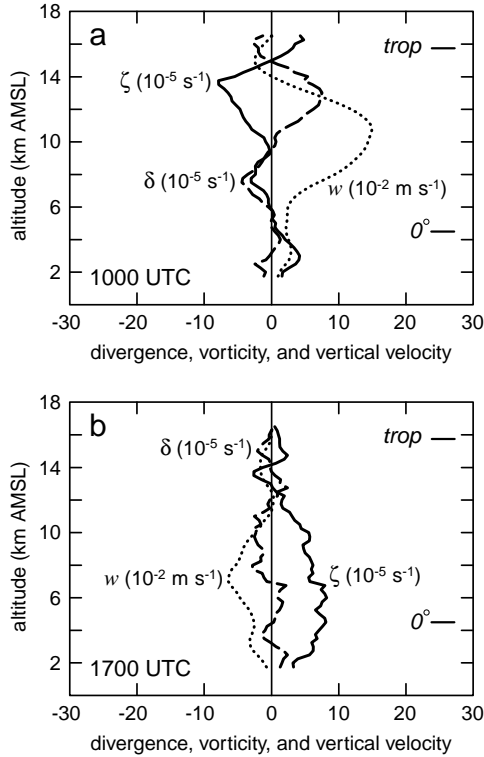


Figure 5: Relative vorticity (solid in 10^{-5} s^{-1}), horizontal divergence (dashed in 10^{-5} s^{-1}), and vertical velocity (dotted in 10^{-2} m s^{-1}) of the total wind at a) 1000 and b) 1700 UTC on 1 August 1996. Profiles are for a $2^\circ \times 2^\circ$ area centered on the MCV in the middle troposphere. Unlike in figure 4, profiles are not for 3-h averages. The levels of 0°C in the environment and of the tropopause are marked along the right side of each panel.

The great depth of the MCV from 1500 to 1800 UTC has precedence. The simulated MCV of Chen and Frank (1993) had a top near 200 hPa, which would be 12.4 km AMSL in our case. The observed MCVs of Brandes (1990) and Bousquet and Chong (2000) had tops near 11 km AMSL.

Acknowledgments. The National Science Foundation supported this research with grants ATM 9618684 and ATM 0071371, the National Aeronautics and Space Administration with grant NCC5-288 SUPP 0002.

REFERENCES

- Barnes, S. L., 1973: Mesoscale objective analysis using weighted time-series observations. NOAA Tech. Memo. ERL NSSL-62, National Severe Storms Laboratory, Norman, OK, 60 pp. [NTIS COM-73-10781. Available from National Severe Storms Laboratory, Norman, OK 73069.]
- Bousquet, O., and M. Chong, 2000: The oceanic mesoscale convective system and associated mesovortex observed 12 December 1992 during TOGA-COARE. *Quart. J. Roy. Meteor. Soc.*, **126**, 189–211.
- Brandes, E. A., 1990: Evolution and structure of the 6–7 May 1985 mesoscale convective system and associated vortex. *Mon. Wea. Rev.*, **118**, 109–127. [See also Corrigendum, 1990: *Mon. Wea. Rev.*, **118**, 990.]
- Chen, S. S., and W. M. Frank, 1993: A numerical study of the genesis of extratropical convective mesovortices. Part I: Evolution and dynamics. *J. Atmos. Sci.*, **50**, 2401–2426.
- Cotton, W. R., M. S. Lin, R. L. McAnelly, and C. J. Tremback, 1989: A composite model of mesoscale convective complexes. *Mon. Wea. Rev.*, **117**, 765–783.
- Hertenstein, R. F. A., and W. H. Schubert, 1991: Potential vorticity anomalies associated with squall lines. *Mon. Wea. Rev.*, **119**, 1663–1672.
- Houze, R. A., Jr., S. A. Rutledge, M. I. Biggerstaff, and B. F. Smull, 1989: Interpretation of Doppler weather radar displays of midlatitude mesoscale convective systems. *Bull. Amer. Meteor. Soc.*, **70**, 608–619.
- Koch, S. E., M. DesJardins, and P. J. Kocin, 1983: An interactive Barnes objective map analysis scheme for use with satellite and conventional data. *J. Climate Appl. Meteor.*, **22**, 1487–1503.
- Maddox, R. A., 1980: An objective technique for separating macroscale and mesoscale features in meteorological data. *Mon. Wea. Rev.*, **108**, 1108–1121.
- Maddox, R. A., D. J. Perkey, and J. M. Fritsch, 1981: Evolution of upper tropospheric features during the development of a mesoscale convective complex. *J. Atmos. Sci.*, **38**, 1664–1674.
- Mapes, B. E., 1993: Gregarious tropical convection. *J. Atmos. Sci.*, **50**, 2026–2037.
- Menard, R. D., and J. M. Fritsch, 1989: A mesoscale convective complex-generated inertially stable warm core vortex. *Mon. Wea. Rev.*, **117**, 1237–1261.
- O'Brien, J. J., 1970: Alternative solutions to the classical vertical velocity problem. *J. Appl. Meteor.*, **9**, 197–203.
- Pandya, R. E., and D. R. Durran, 1996: The influence of convectively generated thermal forcing on the mesoscale circulation around squall lines. *J. Atmos. Sci.*, **53**, 2924–2951.
- Scott, J. D., and S. A. Rutledge, 1995: Doppler radar observations of an asymmetric MCS and associated vortex couplet. *Mon. Wea. Rev.*, **123**, 3437–3457.
- Skamarock, W. C., M. L. Weisman, and J. B. Klemp, 1994: Three-dimensional evolution of simulated long-lived squall lines. *J. Atmos. Sci.*, **51**, 2563–2584.
- Trier, S. B., C. A. Davis, and J. D. Tuttle, 2000: Long-lived mesoconvective vortices and their environment. Part I: Observations from the central United States during the 1998 warm season. *Mon. Wea. Rev.*, **128**, 3376–3395.
- Zhang, D.-L., and J. M. Fritsch, 1988: A numerical investigation of a convectively generated, inertially stable, extratropical warm-core mesovortex over land. Part I: Structure and evolution. *Mon. Wea. Rev.*, **116**, 2660–2687.